Dalton Transactions

The role of titanium-oxo clusters in sulfate production of TiO2

Journal:	*Dalton Transactions*
Manuscript ID	DT-ART-03-2019-001337.R4
Article Type:	Paper
Date Submitted by the Author:	17-Jun-2019
Complete List of Authors:	Kozma, Karoly; Oregon State University, Chemistry Wang , Maoyu; Oregon State University, School of Chemical, Biological, and Environmental Engineering Molina, Pedro; Oregon State University martin, Nicolas; Oregon State University, Chemistry Feng, Zhenxing; Oregon State University, School of Chemical, Biological, and Environmental Engineering; Nyman, May; Oregon State University, Chemistry

ARTICLE

The role of titanium-oxo clusters in sulfate production of TiO_2

Karoly Kozma,[a] Maoyu Wang,[b] Pedro I. Molina,[a,c] Nicolas P. Martin,[a] Zhenxing Feng[b] and May Nyman*[a]

Received 00th January 20xx,
Accepted 00th January 20xx

DOI: 10.1039/x0xx00000x

TiO_2 is manufactured for white pigments, solar cells, self-cleaning surfaces and devices, and other photocatalytic applications. One industrial synthesis of TiO_2 entails: 1) dissolution of ilmenite ore ($FeTiO_3$) in aqueous sulfuric acid which precipitates the Fe while retaining the Ti in solution, followed by 2) dilution or heating the Ti sulfate solution to precipitate the pure form of TiO_2. The underlying chemistry of these processing steps remain poorly understood. Here we show dissolution of a simple Ti^{IV}-sulfate salt, representative of the industrial sulfate production of TiO_2, immediately self-assembles into a soluble Ti-octadecameric cluster, denoted $\{Ti_{18}\}$. We observed $\{Ti_{18}\}$ in solution by small-angle X-ray scattering and Ti extended X-ray absorption fine structure (Ti-EXAFS), and ultimately crystallized it for absolute identification. The $\{Ti_{18}\}$ metal-oxo cluster was prior-reported as a polycation; but shown here, it can also be a polyanion, dependent on the number of sulfate ligands it carries. After immediate self-assembly, the $\{Ti_{18}\}$-cluster persists until TiO_2 precipitates, with no easily identified structural intermediates in solution or solid-state; despite the fact that the atomic arrangement of $\{Ti_{18}\}$ differs vastly from that of titania. The evolution from solution phase $\{Ti_{18}\}$ to precipitated TiO_2 nanoparticles was detailed by X-ray scattering, and Ti-EXAFS. We offer a hypothesis for the key mechanism of complete separation of Fe from Ti in the industrial sulfate process. These findings also highlight the emerging importance of the unusual $Ti(Ti)_5$ pentagonal building unit, featured in $\{Ti_{18}\}$ as well as other early d^0 transition metal chemistries including Nb, Mo and W. Finally, this study presents an example of crystal growth mechanisms in which the observed 'pre-nucleation cluster' does not necessarily predicate the structure of the precipitated solid.

Introduction

Titanium dioxide and titanates have been studied since Fujishima and Honda demonstrated the photooxidation behavior of simple and earth abundant TiO_2. [1] Since this initial discovery, titanium-dioxide forms have been synthesized, doped, and engineered to understand form-function relationships, and to improve the catalytic efficacy[2–5]. Titania is an ideal white pigment, in addition to photocatalyst[6,7]. It is utilized in self-cleaning surfaces (nanomaterial forms) or scaffolding on buildings for degradation of air pollutants[6–9]. Titanium is the second most abundant transition metal in the geosphere; its oxide materials are very stable and considered as low toxicity materials[10]. These industrially important oxides are produced in water, but the Ti-speciation and the influence of solution conditions on the formed material has not been well-elucidated[11].

One process to obtain titanium dioxide is from sulfuric acid solutions at elevated temperature[12]. This sulfate process uses ilmenite ($FeTiO_3$), the most earth-abundant source of titanium. After removing iron by precipitation, TiO_2 is obtained from the remaining titanium sulfate solution. The ore source and the applied methodology determines product purity. Also, physical parameters (e.g. color) of the produced TiO_2 depend on the conditions that promote Fe/Ti separation. Hence, investigations of relevant titanium sulfate solutions are important to optimize this industrial process. In prior studies, Raman-spectroscopy was utilized to characterize speciation, and all reports hypothesized aqua or sulfato coordination complexes of titanyl monomers (TiO^{2+})[11,13,14]. Formation of larger species like titanium-oxo clusters (TOC) was speculated in the process of nucleating TiO_2, but mechanisms and reaction pathways are not understood[14–17].

Metal-oxo clusters, which can be considered molecular metal oxides, are useful models to understand solution processes; in particular, incipient precipitation and crystallization of the related oxide phases.[18] These clusters are sometimes isolated as stable entities without organic ligands; in particular the aluminum polycations[19,20] and the transition metal (Group V/VI) polyoxometalates.[21–23] However, most metal-oxo cluster intermediates must be stabilized by organic ligands for isolation. Nonetheless, even ligated clusters are useful structural models to understand self-assembly processes, and

[a] Department of Chemistry, Oregon State University, 153 Gilbert Hall, Corvallis, OR 97331, USA
[b] School of Chemical, Biological and Environmental Engineering, Oregon State University, Corvallis, OR 97331, USA
[c] Current address: Valliscor, Advanced Technology & Manufacturing Institute, 111- NE Circle Blvd, Corvallis, OR 97330, USA
*Corresponding author. E-mail address: May.Nyman@oregonstate.edu
Electronic Supplementary Information (ESI) available: [details of any supplementary information available should be included here]. See DOI: 10.1039/x0xx00000x

to perform experiments to determine their relevancy on the reaction pathway from monomer to metal oxide[24,25]. Group IV metal-oxo clusters, including Ti^{IV} [26], are an emerging class of inorganic (meaning without organic ligation) aqueous polycations[27–31], and even polyanions[32–34]. Only recently, Wang *et al.* has pioneered the expansion of aqueous TOCs[35]. Several TOCs have been reported with different nuclearity[26,36–39] including $\{Ti_4\}$, $\{Ti_6\}$, $\{Ti_8\}$, $\{Ti_{18}\}$ and heterometallic $\{Ti_{22}Bi_6\}$[40] with respectively 4, 6, 8, 18 or 22 titanium polyhedra ligated with only O^{2-}, OH^- and H_2O (and sulfate in some cases). One of the most fascinating compounds exhibits pentagonal bipyramid coordination ($\{Ti_{18}\}$-cluster), in addition to the common octahedral geometry. This cluster is a stack of three $Ti(Ti)_5$ pentagonal units (**Figure 1b**) in which the pentagonal bipyramid shares five edges with Ti-octahedra in a planar arrangement. Similar units have been also observed in polyoxometalate clusters of Nb[41], Mo[42] and W[43]. The recent discovery of purely inorganic, water-soluble TOCs brings forth opportunity to synthesize and design new titanates with controlled chemical and structural composition through the reaction.

Here we show that in $TiOSO_4$ solutions representative of those employed in TiO_2 production, $\{Ti_{18}\}$ is the dominant specie. This hypothesis was formulated from corroborative solution-characterization techniques including small-angle X-ray scattering (SAXS), pair distribution function (PDF) analysis of X-ray total scattering, and titanium extended X-ray absorption fine structure (Ti-EXAFS). Ultimately crystallization of $\{Ti_{18}\}$ supported this hypothesis. We also tracked to evolution from solution-phase $\{Ti_{18}\}$ to precipitated TiO_2. Intriguingly, we cannot identify the structural intermediate between $\{Ti_{18}\}$ and TiO_2, suggesting rapid conversion. Nonetheless, observed rapid self-assembly of a Ti-cluster that cannot accommodate heteroatoms provides one underpinning mechanism for Fe/Ti separations, and other important metal-metal separations in industry.

Experimental

Reagents and solution preparation

Titanium(IV) oxysulfate, $TiOSO_4 \cdot nH_2O$ (Ti≥99%) and tetrabutylammonium chloride, $N(C_4H_9)_4Cl$ (TBA-Cl) (≥97%) were purchased from Sigma-Aldrich. Concentrated H_2SO_4 was purchased from Macron Fine Chemicals. We also used $TiCl_4$ (99%) for control experiments purchased from Beantown Chemicals. The materials were used as received. Deionized (DI) water (18.2 MΩ, Millipore) was used to prepare all solutions. Solutions for EXAFS, SAXS and PDF measurements were prepared by adding a predetermined amount of $TiOSO_4$ to deionized water and stirring vigorously for 3-4 hours at room temperature to ensure complete dissolution. Note: these solutions cannot be heated, because they yield anatase, per the industrial process.

Crystallization

$\{Ti_{18}\}$-cluster: In order to validate that $TiOSO_4$ solution is dominated by $\{Ti_{18}\}$ and provide control samples for the EXAFS studies, we crystallized $\{Ti_{18}\}$ by employing tetrabutylammonium ion (TBA^+). We dissolved 800 mg $TiOSO_4$ in 5 mL DI water and added 1.39 g TBA-Cl. After complete dissolution, the solution was filtered through a 0.45 µm nylon mesh syringe filter. Colorless crystals appeared after twelve days.

Characterization methods

Detailed description of techniques, experimental parameters and data processing and interpretation is provided in the Electronic Supplementary Information and summarized here. SAXS data were collected on SAXSess instrument (Anton Paar) to obtain information about the dispersity and the size of the species present in solution. The local coordination environments were probed by Ti K-edge extended X-ray absorption fine structure (EXAFS) analysis at 5BM and 20 BM of the Advanced Photon Source (APS) at Argonne National Laboratory (ANL). Single-crystal X-ray diffraction proved identification of clusters observed in solution, and these details of data collection and structure solution and refinement are summarized in the ESI. We performed X-ray total scattering measurements to perform pair distribution function (PDF) analysis with a Rigaku Smartlab X-ray diffractometer (Mo-Kα radiation). Transmission electron microscopy (TEM) images were acquired using a high angle annual dark field detector on an FEI Titan TEM operated at 200 keV in STEM mode. Energy dispersive X-ray spectroscopy (EDX) measurements were performed on Quanta 600 scanning electron microscopy (SEM).

Results and discussion

Solution behavior and solution characterization by X-ray scattering techniques

Representative structures of the key phases of this study, $TiOSO_4 \cdot H_2O$, $\{Ti_{18}\}$ and anatase TiO_2 are shown in **Figure 1**. Briefly, $TiOSO_4 \cdot H_2O$ is a framework structure containing zigzag chains of TiO_6-octahedra along the b-axis. The octahedra are corner-linked by oxo-ligands in a cis-configuration. Three bonds to Ti are from the sulfates, and remaining bond of hexacoordinate Ti is to a terminal water molecule. Each SO_4-tetrahedron bridges four TiO_6-octahedra. The $\{Ti_{18}\}$ cluster is a stack of three pentagonal $Ti(Ti)_5$ units. Within the cluster core, there are 27 oxo ligands; five within each layer around the equatorial belt of the pentagonal bipyramid (edge-sharing) and six that link each set of two layers together (corner-sharing). Terminal ligands are water molecules, and BVS suggests there are no hydroxyl ligands present in the various formulations of $\{Ti_{18}\}$. The five Ti-octahedra of the middle layer have two terminal water molecules each, while the octahedra of the cap layers have varying degrees of replacement of two water ligands by a bridging sulfate ligand around the perimeter of the

pentagonal units, or one water ligand replaced by a terminally-bound sulfate on the pentagon face. The degree of replacement varies in different crystalline lattices[35]. Like most Ti-oxo phases, anatase contains only Ti-octahedra. In **Figure 1**, the Ti-octahedra in the center of the unit cell is highlighted as semi-transparent; all Ti are crystallographically equivalent in anatase. Each octahedron links to four others by edge-sharing (solid polyhedra, **Figure 1**) and four by corner-sharing (not shown). Each oxo ligand bridges three Ti-octahedra.

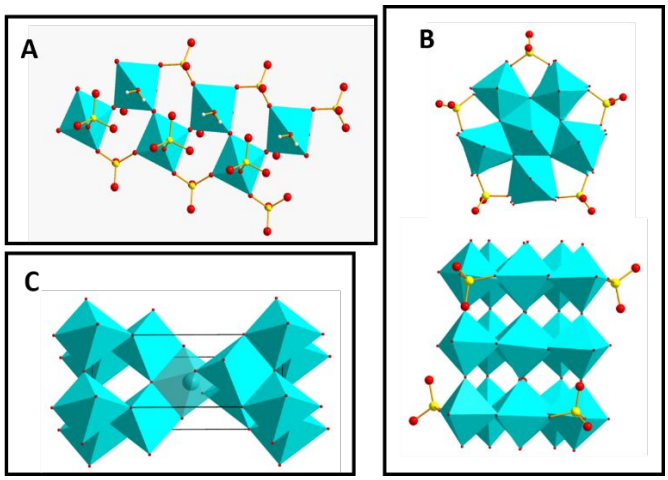

Figure 1 Representations of the relevant structures in this study. A is $TiOSO_4 \cdot H_2O$, B shows two views of a $\{Ti_{18}\}$ cluster; and C shows the unit cell of anatase. Turquoise polyhedra are Ti-centered, red spheres are oxo or water ligands, yellow spheres are sulfur in sulfate anions, and white spheres are hydrogen, of water molecules (in $TiOSO_4 \cdot H_2O$ only).

$TiOSO_4$ (for brevity, will name without hydration henceforth) dissolves in water after several hours of vigorous stirring. Somewhat non-intuitive, solubility increases with concentration. Solutions must have a concentration of 0.2 M or greater, otherwise hydrolysis reactions overcome the dissolution process. This is because the self-buffering behavior of the Ti^{IV}-centers (bound water deprotonates) yields acidic solutions, which retains solubility, and acidity scales with concentration. The pH for solutions of 0.25 - 1.0 M $TiOSO_4$ is summarized in **Table 1.** SAXS curves of these solutions (**Figure 2**) scaled to match in the flat plateau region (q<0.1 $Å^{-1}$) emphasizes the difference in the Guinier region (q=0.1-0.5$Å^{-1}$), demonstrating that cluster size becomes slightly smaller with increasing concentration, evidenced by the shift in the Guinier region to higher q-value. The flat plateau at lower q-values indicates that solutions contain approximately spherical, monodisperse particles with no evidence of aggregation (would exhibit a negative slope) or ordering (would exhibit a positive slope) in solution. The simulated scattering curve for $\{Ti_{18}\}$ matches remarkably well with the experimental scattering curves, up to q=0.6 $Å^{-1}$. The deviation from this match, above q>0.6 $Å^{-1}$ increases with higher concentration and could be due to the presence of small species such as monomers, or some beam attenuation with increasing dissolved species. Additionally, Ti with 22 electrons scatters only moderately better than the S of the sulfate (16 electrons); wherein the sulfate, if not bonded to the cluster, contributes to the background scattering in the high-q region of the curve. Nonetheless, the SAXS data suggests dissolved $TiOSO_4$ could be predominantly $\{Ti_{18}\}$.

Mathematical analysis of the scattering curves provides more quantitative evidence that dissolved $TiOSO_4$ spontaneously self-assembles into $\{Ti_{18}\}$. The radius of gyration (R_g; the shape independent, root mean weighted average of scattering vectors through the scattering particle) for the three solutions are summarized in **Table 1**, along with the R_g from simulated $\{Ti_{18}\}$[44,45]. The R_g for simulated $\{Ti_{18}\}$ matches precisely that of 0.5 M $TiOSO_4$, while the 0.25 M solution has slightly larger average cluster size, and the 1.0 M solution has smaller average cluster size. We also compare the pair distance distribution function (PDDF; probability histogram of scattering vectors through the cluster) of the 0.5 M $TiOSO_4$ solution to that from simulated $\{Ti_{18}\}$, and these also exhibit a good match (**Figure 2**). The maximum linear extent of the simulated and experimental PDDF, where the probability of scattering intensity goes to zero, is 13.8 Å. This is consistent with various measured distanced across the cluster which range from ~12-16 Å; depending on the direction through the cylindrical cluster.

Table 1 Summary of SAXS analysis of $TiOSO_4$ solutions

Sample	pH	R_g (Å) (Guinier-fit)
[Ti]=0.25M	1.40	5.8
[Ti]=0.50M	1.05	5.4
[Ti]=1.0M	0.77	4.9
[Ti]=0.50M, 1M HNO_3	< 0.5	4.1 (ref [40])
$\{Ti_{18}\}$ (simulated)	N/A	5.3
$Ti(Ti)_5$-pentagon (simulated)	N/A	4.1
$\{Ti_4\}$ with sulfate / without sulfate (simulated)	N/A	4.3 / 3.5 (ref [36])
$\{Ti_6\}$ (simulated)	N/A	4.2 (ref [46])
$\{Ti_8\}$ (simulated)	N/A	4.8 (ref [39])

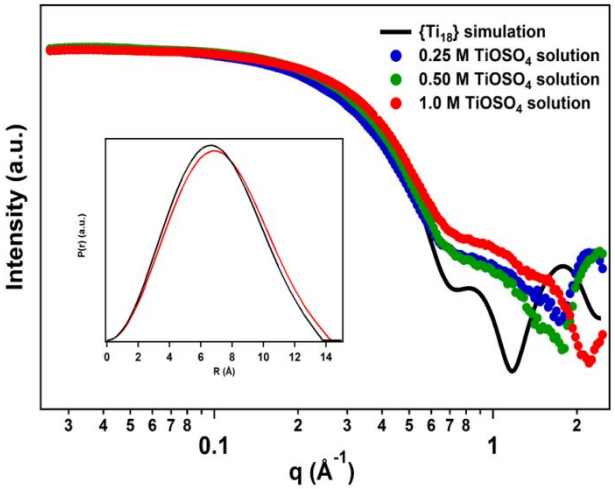

Figure 2 SAXS curves of freshly dissolved $TiOSO_4$ solutions (the curves are scaled to compare the Guinier region). The simulated curve for $\{Ti_{18}\}$-cluster is presented for comparison. Inset: pair distance distribution function (PDDF) analysis of $TiOSO_4$ solution (0.5 M, red) and simulated $\{Ti_{18}\}$-cluster (black).

We suggest the slightly larger R_g for the 0.25 molar solution indicates some hydrolysis reactions linking clusters are initiated. In contrast, $\{Ti_{18}\}$ in the 1.0 M solution may be 'losing' layers. An organically ligated cluster featuring a $\{Ti_{12}\}$ unit (minus one

layer) has very recently been isolated[47]. Dissolving $TiOSO_4$ in acid instead of neat water leads to a significant decrease in the size of scattering species. Prior we observed a 4.1 Å R_g in 0.5M $TiOSO_4$ in 1M HNO_3 solution[40], corresponding precisely with that of the simulated single pentamer unit. We assume increasing acid concentration may hinder stacking of the $Ti(Ti)_5$-pentamers or even formation of the pentamer. On the other hand, we cannot rule out formation of other, water-soluble small sulfate-decorated TOCs with similar size in that acidic media, for instance, the sulfate-decorated $\{Ti_4\}$-cluster[36] (**Table 1**). The I_0-intensity of the non-scaled scattering curves in not linearly-correlated with concentrations, indicating the cluster size is decreasing with increasing concentration (**Figure S1**).

$TiOSO_4$ solution structure by EXAFS

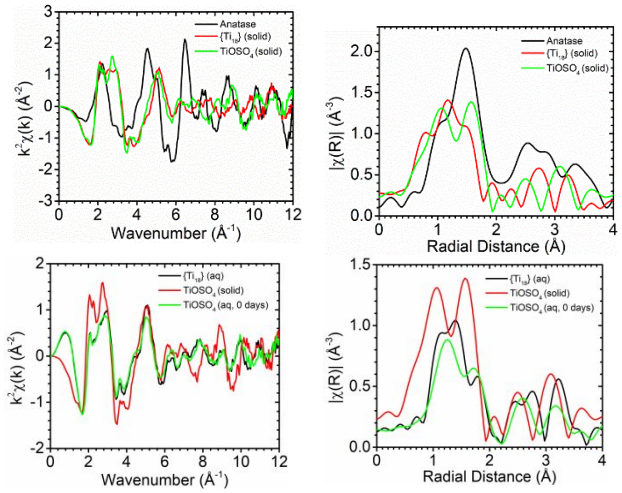

Figure 3 Ti EXAFS k-space (left) and Fourier-transformed R-space (right) of TiO_2 anatase, solid and dissolved $\{Ti_{18}\}$ and $TiOSO_4{\cdot}H_2O$.

Ti K-edge EXAFS[48–54] provided atomic-level information about both solutions and solids for this study. The k-space and R-space data of Ti solids (TiO_2 anatase, crystallized and dissolved $\{Ti_{18}\}$, and $TiOSO_4{\cdot}H_2O$, **Figure 3**), benchmarks atomic-level structural differences between the three materials. Model-based fitting of the Ti K-edge data out to 4 Å in $TiOSO_4$ and $\{Ti_{18}\}$ were well-reproduced (**Figure S2**) by using scattering paths from $TiOSO_4$ and $\{Ti_{18}\}$ crystal structure models (see also **Figures S3-6** for relevant bond distances).

In contrast, the k and R-space EXAFS spectra of aqueous $TiOSO_4$ differs from the solid $TiOSO_4$, but looks similar to crystallized and redissolved $\{Ti_{18}\}$ (**Figure 3**). Quantitative analysis shows that the first shell (R < 2 Å) Ti-O coordination numbers (CNs) for $TiOSO_4$ solution (3.8), and $\{Ti_{18}\}$ solution (3.6) are both considerably less than that of the solids (both defined as 6.00, see **Table S1**), and less than what we expect for octahedral and pentagonal bipyramidal Ti. The decrease of total coordination number from the EXAFS model in the dissolved Ti-species is likely due to ligand lability of the dissolved species. On the other hand, the k-space EXAFS spectrum of redissolved, crystallized $\{Ti_{18}\}$ (discussed below) is nearly identical to that of dissolved $TiOSO_4$, strongly suggesting dissolved $TiOSO_4$ assembles into $\{Ti_{18}\}$ clusters, in agreement with the SAXS data.

There are some differences between the R-space of dissolved $TiOSO_4$ and redissolved $\{Ti_{18}\}$. As discussed below, the only way $\{Ti_{18}\}$ can be crystallized is with tetrabutylammonium (TBA) and chloride counterions and co-ions. The peak(s) in the R-space between 3-4 Å correspond to Ti-Ti and Ti-S pairs within the sulfate-capped $\{Ti_{18}\}$ (see **Figure S4-6**). This peak is more pronounced in the crystallized and dissolved $\{Ti_{18}\}$, likely due to stabilization of decorating sulfate ligands by the TBA and Cl^- ions in solution. The number of sulfates with which $\{Ti_{18}\}$ has been crystallized is variable (discussed below), suggesting this ligand is labile in solution. Similarly, there are more pronounced peaks for $\{Ti_{18}\}$, corresponding with Ti-O pairs (1-2 Å) and around R=2.8 Å, corresponding with distal Ti-O distances in the cluster and/or substitution of Cl^- for H_2O or sulfate.

Single crystal structural description

We attempted to isolate the dominant cluster form from $TiOSO_4$ solutions for absolute identification. Adding different counter ions and crystallization agents (e.g. alkali ions, tetraalkylammonium ions or γ-cyclodextrin) and employing different crystallization methods (solvent evaporation, solvent diffusion) were not successful. The prior-reported and crystallized $\{Ti_{18}\}$ was obtained from a mixture of $TiCl_4$ and sulfuric acid (crystallized with tetrabutylammonium, TBA^+)[35]. To include all the same ions, we added TBA-Cl to a solution of $TiOSO_4$ (1.0 M; see experimental) and obtained crystals by slow solvent evaporation. The average formulation in the final refined structure is $[Ti_{18}O_{27}(H_2O)_{25}(SO_4)_{9.5}](Cl)_5(TBA)_6{\cdot}13.5H_2O$ (**Figure 4**). Due to twinning and significant disorder in every crystal we analysed, the refined X-ray data is of sub-optimal quality. However, it served two important functions: 1) the $\{Ti_{18}\}$ core is clearly observed, despite the disorder of solvent, counterions and sulfate; and 2) *because* of the disordered and presumably labile sulfate observed in the structure, we can explain the very high solubility of this cluster in water, despite its relatively low ionic charge. These points are discussed below. The X-ray structure provides strong evidence that $TiOSO_4$ self-assembles into $\{Ti_{18}\}$ immediately upon dissolution as observed by SAXS. Moreover, isolation of $\{Ti_{18}\}$ from solution also enabled the comparative EXAFS studies described above. The average formulation of the cluster core including the sulfates is very close to neutral, $[Ti_{18}O_{27}(SO_4)_{9.5}]^{1-}$. In solution and the crystallized solid, there is likely a labile mixture of neutral clusters plus clusters with a small negative charge and clusters with a small positive charge. This both enables the high solubility and the lack of observed structure factor (ordering in solution) in SAXS data, since there should be minimal repulsion between clusters with a charge range of -1 to +1. Details of the sulfate-chloride disorders are described and illustrated in the ESI. Five different compositional variations of $\{Ti_{18}\}$ were reported prior, based on number and location of decorating sulfate or selenate anions. These included six, eight and nine sulfate/selenate anions, with respective charge of 4+, 2+, and 0. This prior and currently observed variation of sulfate ligation strengthens the argument that a mixture of polyanions and polycations coexist in dissolved $TiOSO_4$.

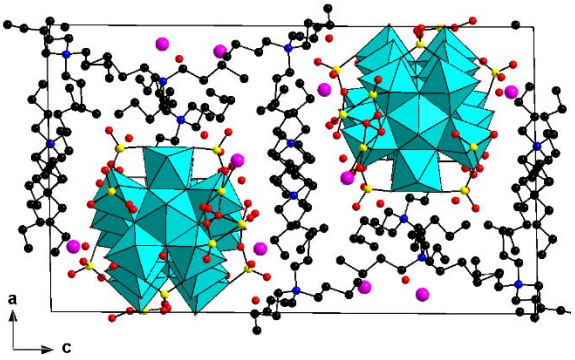

Figure 4 Unit cell view of crystallized $\{Ti_{18}\}$, illustrating close association of Cl^- with the cluster. Ti-polyhedra are turquoise, sulfates are yellow and red ball-and-stick, Cl^- are pink spheres, TBA are black (C) and blue (N) spheres.

Aging of $TiOSO_4$ solutions

Per the industrial sulfate process, titanium sulfate solutions preciptate anatase TiO_2 upon dilution or heating [55]. In this study, aging $TiOSO_4$ solutions at ambient conditions also produced anatase-TiO_2, but the process is significantly slower. For 0.25M $TiOSO_4$, precipitation appears after 6 days, while the solid product is apparent at around 45 days of aging the 1.0 M solution. Higher concentration of $[Ti^{4+}]$ implies higher $[H^+]$ concentration (**Table 1**), suppressing hydrolysis and condensation reactions. Contrarily, decreased Ti-concentration accelerates TiO_2 formation. We prepared several 0.25 M $TiOSO_4$ solutions and collected the solid product in the 6-80 day time-period to determine a yield approaching 50% in approximately 3 months (**Figure S10**). We could collect enough solid product for further characterization after 21 days. Despite the poor crystallinity of the obtained precipitate shown by the X-ray total scattering curve, PDF analysis of that curve confirmed formation of TiO_2 anatase phase (**Figure 5)**. Additionally, the observed particle size is 1.96 nm using a spherical nanoparticle model for refinement by PDFGui[56] (**Table S3**), in good agreement with TEM analysis (**Figure 5A**). EDX indicated the formation of sulfate-decorated anatase nanoparticles with 1:4 S:Ti ratio (**Figure S11**). We will address the structural evolution of the precipitated titanium oxide phase in the near future.

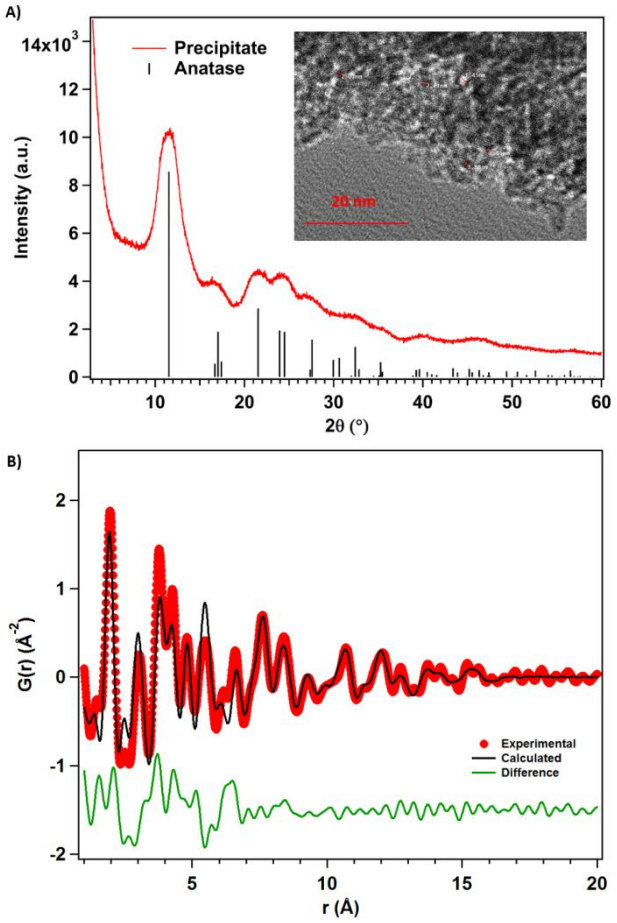

Figure 5 A: X-ray total scattering pattern of the precipitated solid from 0.25M $TiOSO_4$ solution after 21 days. The broad peaks (indicating low crystallinity) are good agreement with the calculated peak positions of TiO_2 anatase phase (black). (Note: Mo Kα radiation was used, where λ=0.71 Å.) Inset: TEM image of precipitate. Red lines correspond with particle size of 2.07, 2.21, 1.45, 1.88, 2.05 and 1.45 nm. B: Experimental PDF analysis of the X-ray total scattering curve. Atom-pair correlations are in good agreement with anatase phase with approximately 2.0 nm particle size.

SAXS shows that $\{Ti_{18}\}$ evolves into larger soluble species with $TiOSO_4$ solution aging (**Figs 6 & S12)**. Consistent with the time delay preceding TiO_2 precipitation, formation of this species is slower in higher concentration $TiOSO_4$ solutions. Intriguingly, the new species also has a distinct size, suggesting it could also be a TOC molecular cluster. We used a two-phase model to fit the data, and the four parameters (radius and % population) are summarized in **Table S4**. The second population is roughly twice the size of $\{Ti_{18}\}$ and similar to the TiO_2 nanoparticles that eventually precipitate (~2 nm). This larger specie appears prior to precipitation and its size does not change over time, suggesting it is likewise a molecular titanium-oxo cluster rather than TiO_2 nanoparticles. Additionally, we filtered the solutions immediately before measuring the SAXS data to ensure no colloidal particles are present in the solution. The maximum population of this larger specie is less than 10%, according to the SAXS analysis.

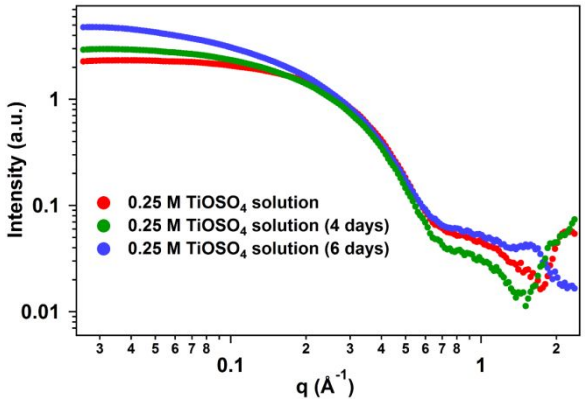

Figure 6 SAXS curves of aged samples of 0.25M $TiOSO_4$ solutions.

While SAXS shows increasing size of TOCs with solution aging, EXAFS reveals this occurs without significant atomic-level structural change within the TOCs **(Figure 7)**. These results suggest the second hypothetical TOC has similar short-range order as $\{Ti_{18}\}$. Zhang et al. recently published two intriguing TOC clusters (organically ligated) that provides a model for joining $\{Ti_{18}\}$ clusters without significantly altering the short-range order[47]. These clusters feature double stacks of the $Ti(Ti)_5$ unit that are linked side-by-side; with or without a 90° rotation. Zhang and coworkers also compared the orientation of Ti in these side-by-side stacks to the arrangement of Ti in brookite and in anatase TiO_2. This recent study taken together with our current results may present a consistent model for the conversion of $Ti(Ti)_5$, $\{Ti_{18}\}$, and related clusters to TiO_2.

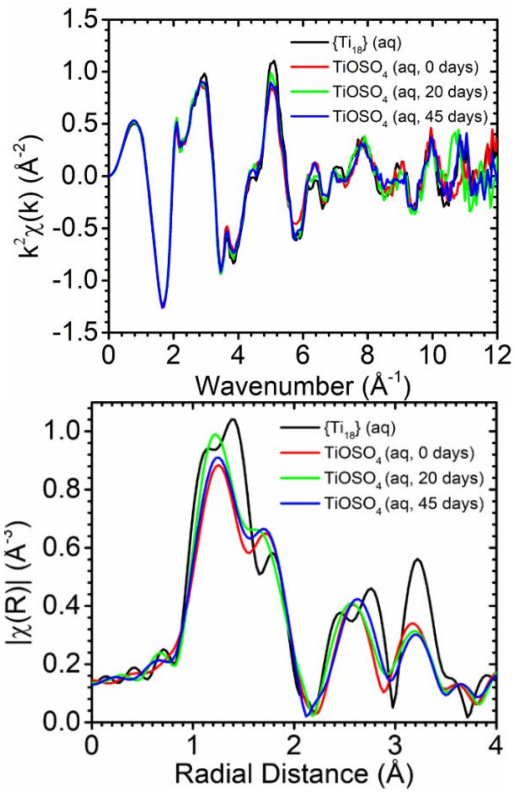

Figure 7 Ti K-edge K-space (top) and R-space (bottom) EXAFS data comparing dissolved $\{Ti_{18}\}$ to dissolved $TiOSO_4$ (fresh and aged; 1M). Differences observed in the R-space data primarily reflect the influences of poor statistics at higher k values.

Conclusions

Here we demonstrate that high solubility of Ti in the sulfate process may be controlled by its speciation as discrete $\{Ti_{18}\}$ polycations that by definition, eliminate heteroatoms such as Fe. Moreover, the $\{Ti_{18}\}$ clusters persist in solution state without structural change, even in equilibrium with precipitating TiO_2. This latter point is particularly remarkable because the atomic and polyhedral arrangements of $\{Ti_{18}\}$ and TiO_2 are profoundly different. This leads to questions about the relevance and role of prenucleation clusters in other simple metal oxide systems such as iron oxides. The unusual pentagonal bipyramidal Ti and pentagonal $Ti(Ti)_5$ unit that is the key foundation and scaffold of $\{Ti_{18}\}$ is becoming more commonly observed since its discovery in 2016[35], even in sulfate-free and non-aqueous conditions[47]. The pentagonal unit, now recognized and even common in multiple early d^0 transition metals (also Mo, W and Nb) inspires understanding of its stability, formation mechanism, and design of new functional metal oxides built of the pentagonal unit. Other ongoing studies include investigating formation of $\{Ti_{18}\}$ in the presence of Fe; relevant to the industrial sulfate process. Finally, we endeavour to understand the atomic level process of conversion of dissolved $\{Ti_{18}\}$ to precipitated TiO_2 from both a computational and experimental prospective.

Conflicts of interest

There are no conflicts to declare.

Acknowledgements

This study was supported by the U.S. Department of Energy, Office of Basic Energy Sciences, Division of Material Sciences and Engineering, under award DE SC0010802.

Special note: The authors of this manuscript accompanying deposited structure CCDC-1898206 are aware that the quality is below that acceptable by *Dalton Transactions*. Because the purpose of the structure was to provide absolute identification of the $[Ti_{18}]$ cluster in $TiOSO_4$ aqueous solutions, we could not optimize crystal growth conditions without significantly altering the original solution conditions. However, the crystal data is sufficient to identify the $[Ti_{18}]$ unit clearly.

References

1 A. Fujishima and K. Honda, *Nature*, 1972, **238**, 37–38.
2 Y. Ma, X. L. Wang, Y. S. Jia, X. B. Chen, H. X. Han and C. Li, *Chem. Rev.*, 2014, **114**, 9987–10043.
3 J. Schneider, M. Matsuoka, M. Takeuchi, J. Zhang, Y. Horiuchi, M. Anpo and D. W. Bahnemann, *Chem. Rev.*, 2014, **114**, 9919–9986.
4 K. Hashimoto, H. Irie and A. Fujishima, *Jpn. J. Appl. Phys.*, 2005, **44**, 8269–8285.
5 F. De Angelis, C. Di Valentin, S. Fantacci, A. Vittadini and A. Selloni, *Chem. Rev.*, 2014, **114**, 9708–9753.

6 Y. Zhang, Z. Jiang, J. Huang, L. Y. Lim, W. Li, J. Deng, D. Gong, Y. Tang, Y. Lai and Z. Chen, *RSC Adv.*, 2015, **5**, 79479–79510.
7 Y. F. Li and Z. P. Liu, *J. Am. Chem. Soc.*, 2011, **133**, 15743–15752.
8 Y. Lan, Y. Lu and Z. Ren, *Nano Energy*, 2013, **2**, 1031–1045.
9 N. Rahimi, R. A. Pax and E. M. A. Gray, *Prog. Solid State Chem.*, 2016, **44**, 86–105.
10 H. Shi, R. Magaye, V. Castranova and J. Zhao, *Part. Fibre Toxicol.*, , DOI:10.1186/1743-8977-10-15.
11 I. Szilágyi, E. Königsberger and P. M. May, *Inorg. Chem.*, 2009, **48**, 2200–2204.
12 W. Zhang, Z. Zhu and C. Y. Cheng, *Hydrometallurgy*, 2011, **108**, 177–188.
13 A. W. Hixson and W. W. Plechner, *Ind. Eng. Chem.*, 1933, **25**, 262–274.
14 W. Wang, Y. Liu, T. Xue, J. Li, D. Chen and T. Qi, *Chem. Eng. Sci.*, 2015, **134**, 196–204.
15 M. Simonsen and E. Søgaard, *Eur. J. Mass Spectrom.*, 2013, **19**, 265–273.
16 E. D. Bøjesen and B. B. Iversen, *CrystEngComm*, 2016, **18**, 8332–8353.
17 M. E. Simonsen and E. G. Søgaard, *J. Sol-Gel Sci. Technol.*, 2010, **53**, 485–497.
18 O. Sadeghi, L. N. Zakharov and M. Nyman, *Science (80-.).*, 2015, **347**, 1359–1362.
19 G. Johansson, *Acta Chem. Scand.*, 1960, **14**, 771–773.
20 W. H. Casey, *Chem. Rev.*, 2006, **106**, 1–16.
21 Pope T. M., *Heteropoly and Isopoly Oxometalates*, 1983.
22 M. Nyman and P. C. Burns, *Chem. Soc. Rev. Chem. Soc. Rev*, 2012, **41**, 7354–7367.
23 W. Wang, M. Amiri, K. Kozma, J. Lu, L. Zakharov and M. Nyman, *Eur. J. Inorg. Chem.*, 2018, **2018**, 4638–4642.
24 C. Falaise, H. A. Neal and M. Nyman, *Inorg. Chem.*, 2017, **56**, 6591–6598.
25 O. Sadeghi, M. Amiri, E. W. Reinheimer and M. Nyman, *Angew. Chemie - Int. Ed.*, 2018, **57**, 6247–6250.
26 W.-H. Fang, L. Zhang and J. Zhang, *Chem. Soc. Rev.*, 2018, **47**, 404–421.
27 P. J. Squattrito, P. R. Rudolf and A. Clearfield, *Inorg. Chem.*, 1987, **26**, 4240–4244.
28 R. E. Ruther, B. M. Baker, J. H. Son, W. H. Casey and M. Nyman, *Inorg. Chem.*, 2014, **53**, 4234–4242.
29 A. Kalaji and L. Soderholm, *Inorg. Chem.*, 2014, **53**, 11252–11260.
30 A. Clearfield and P. A. Vaughan, *Acta Crystallogr.*, 1956, **9**, 555–558.
31 G. M. Muha and P. A. Vaughan, *J. Chem. Phys.*, 1960, **33**, 194–199.
32 A. Kalaji and L. Soderholm, *Chem. Commun.*, 2014, **50**, 997–9.
33 S. Goberna-Ferron, D. H. Park, J. M. Amador, D. A. Keszler and M. Nyman, *Angew. Chemie - Int. Ed.*, 2016, **55**, 6221–6224.
34 B. Chakraborty and I. A. Weinstock, *Coord. Chem. Rev.*, 2019, **382**, 85–102.
35 G. Zhang, C. Liu, D. L. Long, L. Cronin, C. H. Tung and Y. Wang, *J. Am. Chem. Soc.*, 2016, **138**, 11097–11100.
36 G. Zhang, J. Hou, C. H. Tung and Y. Wang, *Inorg. Chem.*, 2016, **55**, 3212–3214.
37 M. Y. Gao, F. Wang, Z. G. Gu, D. X. Zhang, L. Zhang and J. Zhang, *J. Am. Chem. Soc.*, 2016, **138**, 2556–2559.
38 G. Zhang, W. Li, C. Liu, J. Jia, C. H. Tung and Y. Wang, *J. Am. Chem. Soc.*, 2018, **140**, 66–69.
39 B. Y. M. G. Reichmann, F. J. Hollandert and A. T. Bell, *Acta Crystallogr.*, 1987, **17**, 1681–1683.
40 P. I. Molina, K. Kozma, M. Santala, C. Falaise and M. Nyman, *Angew. Chemie - Int. Ed.*, 2017, **56**, 16277–16281.
41 R. Tsunashima, D. L. Long, H. N. Miras, D. Gabb, C. P. Pradeep and L. Cronin, *Angew. Chemie - Int. Ed.*, 2010, **49**, 113–116.
42 A. Müller, P. Kögerler and A. W. M. Dress, *Coord. Chem. Rev.*, 2001, **222**, 193–218.
43 C. Schäffer, A. Merca, H. Bögge, A. M. Todea, M. L. Kistler, T. Liu, R. Thouvenot, P. Gouzerh and A. Müller, *Angew. Chemie - Int. Ed.*, 2009, **48**, 149–153.
44 R. Zhang, P. Thiyagarajan and D. M. Tiede, *J. Appl. Crystallogr.*, 2000, **33**, 565–568.
45 D. M. Tiede, R. Zhang, L. X. Chen, L. Yu and J. S. Lindsey, *J. Am. Chem. Soc.*, 2004, **126**, 14054–14062.
46 G. Zhang, J. Hou, M. Li, C.-H. Tung and Y. Wang, *Inorg. Chem.*, 2016, **55**, 4704–4709.
47 X. Fan, J. Wang, K. Wu, L. Zhang and J. Zhang, *Angew. Chemie Int. Ed.*, 2019, **58**, 1320–1323.
48 T. Miyanaga, I. Watanabe and S. Ikeda, *Bull. Chem. Soc. Jpn.*, 1990, **63**, 3282–3287.
49 D. Lundberg and I. Persson, *J. Solution Chem.*, 2017, **46**, 476–487.
50 Z. Weng, Y. Wu, M. Wang, J. Jiang, K. Yang, S. Huo, X. F. Wang, Q. Ma, G. W. Brudvig, V. S. Batista, Y. Liang, Z. Feng and H. Wang, *Nat. Commun.*, 2018, **9**, 1–9.
51 L. P. Wang, Y. Leconte, Z. Feng, C. Wei, Y. Zhao, Q. Ma, W. Xu, S. Bourrioux, P. Azais, M. Srinivasan and Z. J. Xu, *Adv. Mater.*, , DOI:10.1002/adma.201603286.
52 C. Wei, Z. Feng, M. Baisariyev, L. Yu, L. Zeng, T. Wu, H. Zhao, Y. Huang, M. J. Bedzyk, T. Sritharan and Z. J. Xu, *Chem. Mater.*, 2016, **28**, 4129–4133.
53 C. Wei, Z. Feng, G. G. Scherer, J. Barber, Y. Shao-Horn and Z. J. Xu, *Adv. Mater.*, 2017, **29**, 1–8.
54 Z. Feng, Q. Ma, J. Lu, H. Feng, J. W. Elam, P. C. Stair and M. J. Bedzyk, *RSC Adv.*, 2015, **5**, 103834–103840.
55 A. Pottier, S. Cassaignon, C. Chanéac, F. Villain, E. Tronc and J.-P. Jolivet, *J. Mater. Chem.*, 2003, **13**, 877–882.
56 C. L. Farrow, P. Juhas, J. W. Liu, D. Bryndin, E. S. Božin, J. Bloch, T. Proffen and S. J. L. Billinge, *J. physics. Condens. matter*, 2007, **19**, 335219.